A Novel Soft-Switching Full-Bridge Converter With a Combination of a Secondary Switch and a Nondissipative Snubber

Dai-Duong Tran, Hai-Nam Vu, Sunho Yu, and Woojin Choi, *Member, IEEE*

***Abstract*—In this paper, a novel soft-switching full-bridge converter with an additional secondary switch and a nondissipative energy recovery snubber is proposed. Thanks to the combination of an active switch and the capacitor—diode–diode snubber employed at the secondary side of the converter, the proposed converter can achieve zero-voltage zero-current switching for all of the primary switches and rectifier diodes over the entire load range. As a result, the rectifier diodes have no reverse-recovery problem and their ringing voltage is clamped. In addition, since no phase shift is used for the gate signals of the primary-side switches, the converter control can be implemented easily and it has no circulating current inherently. The converter exhibits a significant improvement in terms of efficiency, especially under light-load conditions, which is difficult to achieve with conventional phase-shift full-bridge converters. A 3-kW prototype circuit is implemented to verify the superior performance of the proposed converter.**

***Index Terms*—Circulating current, nondissipative snubber, soft-switching full-bridge (SSFB) converter, zero-current switching (ZCS) turn off, zero-voltage switching (ZVS) turn on.**

I. Introduction

ISOLATED full-bridge dc–dc converters have been widely used in many applications, such as power supplies, renewable energy systems, energy storage systems, and traction systems for electric vehicles due to their ability to handle high power with a simple topology, easy control, and high efficiency [1], [2]. Unlike hard-switching pulse-width modulation (PWM) converters, phase-shift full-bridge (PSFB) converters, which adopt the phase-shift modulation technique, are more attractive since they have several advantages, such as soft switching of the power switches, reduction of electromagnetic interference, and improvements in power density and efficiency [3]–[5]. Thanks to its soft-switching capability, by using the parasitic components of the switches and the transformer, the switching device can be turned on when the voltage across it is zero. Therefore, the switching loss can be significantly reduced especially in high-power applications. However, PSFB converters also have some drawbacks. First, the soft-switching condition is achieved by a complex PWM switching scheme. Second, PSFB converters suffers from a narrow zero-voltage switching (ZVS) range and low efficiency at light loads. In order to guarantee a wide ZVS range of a switch, the leakage inductance of the transformer needs to be increased. However, this reduces the effective duty and increases the period of the circulating current thereby increasing the loss. The circulating current in the primary side of the transformer is another disadvantage since it increases the conduction loss and decreases the efficiency, especially when the freewheeling interval is prolonged.

To handle the above mentioned issues of PSFB converters, several kinds of remedies have been proposed [6]–[20]. The general principle used to extend the ZVS range is to employ an assistant current source at the primary side to store sufficient inductive energy to discharge the output capacitance of the switches. The current source can be realized by adding a large external inductor connected in series with the transformers [6], or by utilizing the magnetizing inductance of the additional transformer in case of hybrid topologies [8]–[10]. However, this can be achieved at the cost of bulky magnetic components which are accompanied by increases in the duty-cycle loss, volume, cost, and conduction loss of the converter.

Secondary transient overvoltage and circulating current problems are often treated together since the snubbers employed to suppress the transient voltage helps to reduce the circulating current by isolating the secondary rectifier from both the primary circuit and the secondary freewheeling circuit [11]–[20]. In [11], a dissipated *RCD* snubber is employed to mitigate the voltage ringing across the rectifier diodes. However, it is not possible to avoid the additional loss and heat generated at the snubber resistor. In [12]–[15], a switched-capacitor active-clamp snubber was proposed. However, due to an auxiliary driver circuit and an additional inductor, the complexity and component counts of the circuit are increased. A coupled-inductor-based capacitor–diode–diode (CDD) topology was proposed in [16]. This topology successfully reduces the circulating current and achieves the soft-switching condition for the lagging leg switches. However, the circulating current is not completely eliminated and zero-current switching (ZCS) turn off of the leading leg switches is

Manuscript received October 4, 2016; revised December 9, 2016 and February 21, 2017; accepted March 16, 2017. Date of publication March 28, 2017; date of current version November 2, 2017. Recommended for publication by Associate Editor A. Safaee. *(Corresponding author: Woojin Choi.)*

The authors are with the Electrical Engineering Department, Soongsil University, Seoul 156-743, South Korea (e-mail: dai-duong.tran@vub.ac.be; nam.vhn91@gmail.com; hssky2002@naver.com; cwj777@ssu.ac.kr).

Color versions of one or more of the figures in this paper are available online at http://ieeexplore.ieee.org.

Digital Object Identifier 10.1109/TPEL.2017.2688580

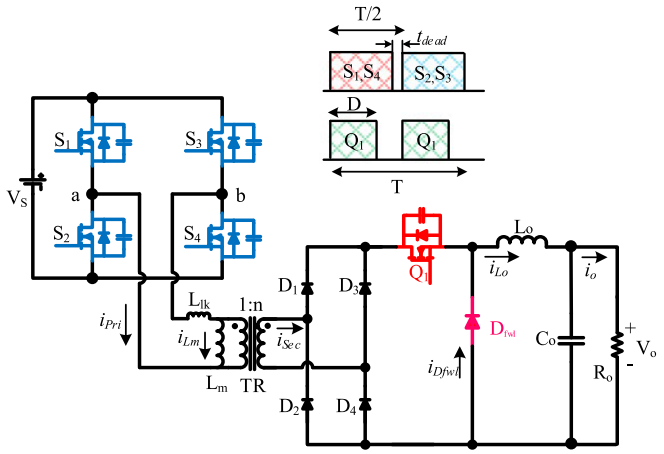

Fig. 1. SSFB converter with a secondary switch and a freewheeling diode [26].

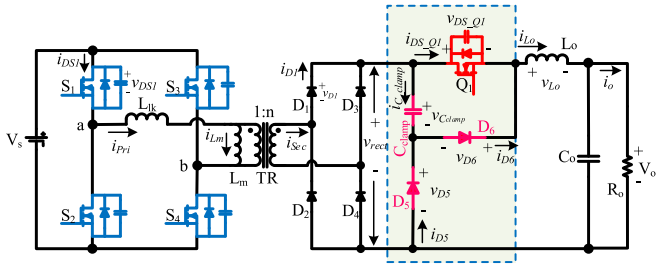

Fig. 2. Proposed SSFB dc–dc converter.

not possible. Generally, most of the proposed methods for PSFB converters so far have been successful in reducing circulating current or extending the soft-switching range at the cost of additional circuits and/or a complicated switching scheme. It is difficult to find a method which can achieve both, and there are no methods that can achieve ZVS turn on and ZCS turn off for all of the primary switches.

A full-bridge converter with a secondary-side phase-shifting active rectifier appears as an alternative approach to achieve both a reduction of the circulating current and full soft switching of the primary switches [23]–[25]. It can be implemented by replacing one leg of the secondary rectifier diodes with active switches to control the output voltage by modulating the phase shift between the primary and secondary switches. In these converters, the primary switches are controlled with a fixed duty cycle (50%) at a constant switching frequency. One challenge in this converter is the complicated design process of the turn-off snubber capacitors for wide load range operation. If designed improperly, the snubber capacitor can resonate with the parasitic inductor of the circuit, which leads to a severe voltage ringing across the switches. In addition, it contributes to a change in the value of the effective capacitance, which limits the ZVS range under the light-load condition. In [25], a saturable inductor is employed in series with the secondary switch to help achieve ZVS of the primary switches by providing the primary side with additional inductive energy. However, it is difficult to select a suitable core for each application, which leads to a complicated circuit design.

With the aforementioned ideas, it is possible to deduce that many advantages of the full-bridge converter can be obtained by employing an additional active switch and a freewheeling diode at the secondary circuit to implement a controlled rectifier and an independent freewheeling current loop. Fig. 1 shows a full-bridge converter with an additional switch and a freewheeling diode at the secondary circuit. The operation of this converter can be summarized as follows. The active secondary switch Q_1 operates at double the primary switching frequency to transfer power to the load, and the output can be regulated by controlling its duty. Since the diagonally opposite switch pairs in the primary side operate with a 180° phase shift, ZVS turn on for all of the primary switches is possible with a small dead time $t_{\rm dead}$ between them. This is mainly due to the energy stored in the magnetizing inductance of the transformer. It can be easily deduced that if the switch Q_1 turns OFF prior to the turn off of the primary switch pair, it can reset the primary current, thereby achieving the ZCS turn-off condition for the primary switch pairs. In addition, circulating current does not exist inherently since no phase shift is introduced in the primary switch control. However, when the switch Q_1 turns OFF, a severe ringing voltage will appear across the switch and rectifier diodes due to resonance between the leakage inductance of the transformer $L_{\rm lk}$ and the effective capacitance of the secondary circuit. Hence, it is necessary to employ a suitable turn-off snubber circuit to alleviate the ringing voltage. Among the different kinds of snubber topologies [11]–[20], a CDD snubber circuit is selected as an appropriate candidate due to its ability to regenerate energy, unless it is otherwise dissipated. An additional benefit obtained by introducing a CDD snubber is that the diodes in the CDD snubber circuit can also be used to provide a path for the freewheeling current, thereby contributing to a reduction in the component count.

In this paper, a novel soft-switching full-bridge (SSFB) dc–dc converter is proposed as shown in Fig. 2. The combination of an additional switch and a CDD snubber is employed in the secondary side of the circuit. The main advantages of the proposed SSFB converter can be summarized as follows:

1) ZVS turn on and ZCS turn off for all of the primary switches over the entire load range;
2) ZVS turn on and ZCS turn off for all of the rectifier diodes and the snubber diode, and the elimination of the reverse-recovery problem;
3) it is inherently free of circulating current and the conduction losses associated with it;
4) no duty-cycle loss due to the immediate energy transfer together with the secondary switch turn on by the clamp capacitor;
5) high efficiency, especially at light loads;
6) simple switching and control schemes.

The comparison between the different kinds of the conventional full-bridge converters and the proposed SSFB converter is shown in Table I.

Details on the operation principle of the proposed SSFB converter are presented in Section II. An analysis of the proposed converter is presented in Section III. A 3-kW hardware prototype has been implemented to verify the performance of the proposed converter. The experimental results presented in

TABLE I
COMPARISON OF THE DIFFERENT KINDS OF FULL-BRIDGE CONVERTERS

(1)	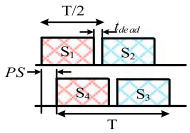 Phase-shift control for primary side switches	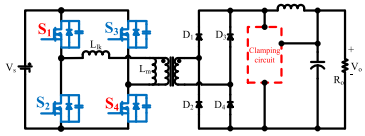 [3]-[16]
	Advantages ▪ ZVS turn-on for primary switches	*Disadvantages* ▪ Complicate switching scheme ▪ Hard switching turn-off for the primary switches ▪ Large circulating current ▪ Limited ZVS range
(2)	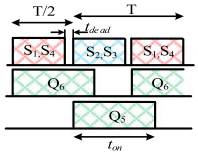 Fixed 50% duty for primary switches, and variable turn-on time for two secondary switches	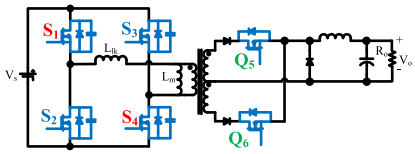 [17]
	Advantages ▪ ZVS turn-on for primary switches ▪ ZCS turn-off for only lagging-leg switches	*Disadvantages* ▪ Complicate switching scheme ▪ Two additional active switches in secondary circuit ▪ Hard switching turn-off for leading leg switches
(3)	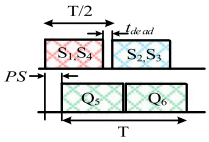 Fixed 50% duty for primary switches, and phase-shift between primary and secondary active switches	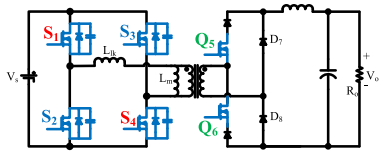 [23]
	Advantages ▪ ZVS turn-on for primary switches ▪ ZCS turn-off for only lagging-leg switches	*Disadvantages* ▪ Complicate switching scheme ▪ Two additional active switches in the secondary circuit ▪ Hard switching turn-off for leading leg switches
(4)	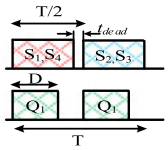 Fixed 50% duty for primary switches and duty control of secondary side switch	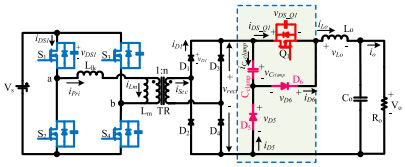 Proposed converter (Developed from [26])
	Advantages ▪ ZVS and ZCS for all primary switches ▪ Soft switching for rectifier diodes and no reverse recovery loss ▪ Simple switching scheme	*Disadvantages* ▪ Hard-switching for additional switches

Section IV show that the proposed converter can achieve high efficiency over the entire load range, especially at a light load.

II. OPERATING PRINCIPLE OF THE PROPOSED SSFB CONVERTER

The operating principle of the proposed SSFB converter in Fig. 3 can be explained by using its key waveforms in Fig. 4. The operation of the proposed converter can be divided into seven modes, and the analysis for each mode of operation is detailed as follows. For the sake of simplicity, it is assumed that all of the circuit components are ideal except the output capacitances of the switches.

Mode 1 [t_0–t_1]*:* In this mode, power is delivered to the load through the switches S_1, S_4, and Q_1. The primary current i_{Pri} is equal to the reflected output inductor current plus the magnetizing current i_{Lm}, and the slope of the output inductor current $\mathrm{i_{Lo}}$ can be calculated by

$$\frac{di_{Lo}}{dt} = \frac{nV_s - V_o}{L_o}. \tag{1}$$

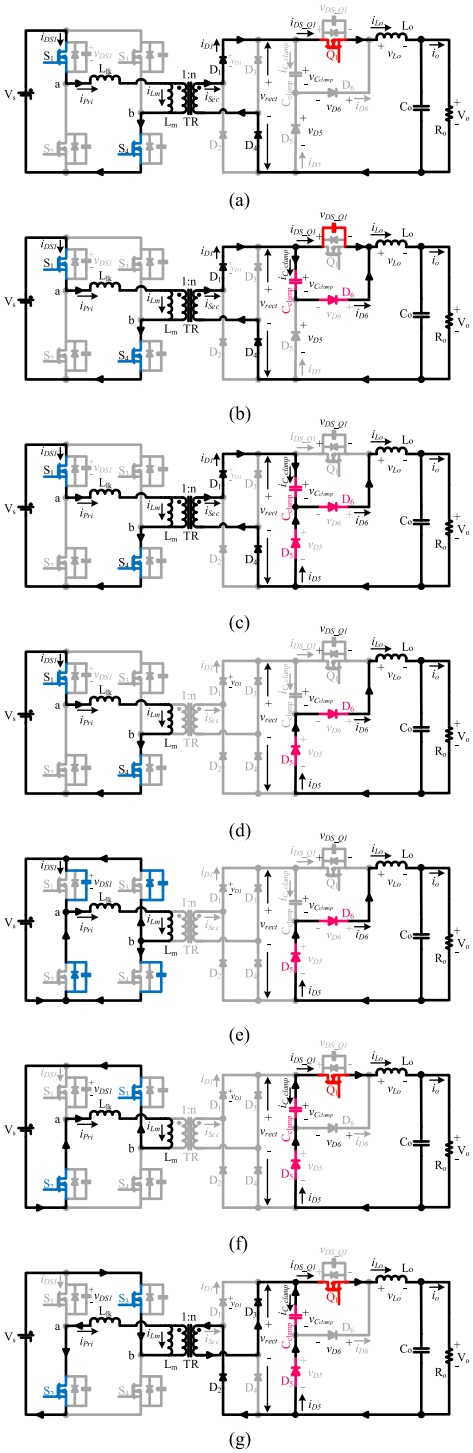

Fig. 3. Modes of operation of the proposed SSFB converter. (a) Mode 1 $[t_0$–$t_1]$. (b) Mode 2 $[t_1$–$t_2]$. (c) Mode 3 $[t_2$–$t_3]$. (d) Mode 4 $[t_3$–$t_4]$. (e) Mode 5 $[t_4$–$t_5]$. (f) Mode 6 $[t_5$–$t_6]$. (g) Mode 7 $[t_6$–$t_7]$.

Mode 2 $[t_1$–$t_2]$: This mode begins with the hard-switching turn off of the secondary side switch Q_1. As soon as the switch Q_1 is turned off, both the output capacitance of the switch Q_1 and the clamping capacitor C_{clamp} start to get charged and to resonate with the primary leakage inductance of the transformer L_{lk} and the output inductor L_o. Since $L_o \gg L_{lk}$ and $C_{\text{clamp}} \gg C_{\text{oss}}$, the resonant frequency of the current can be calculated

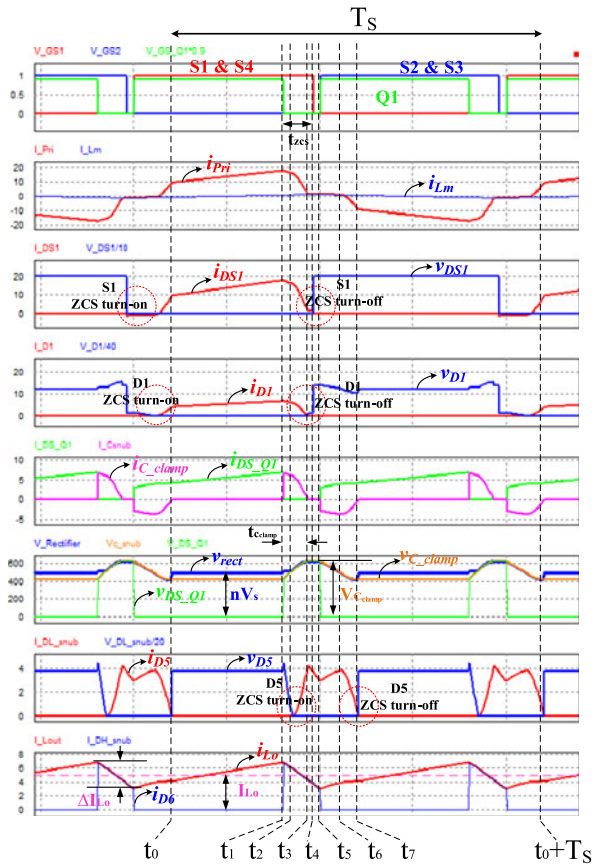

Fig. 4. Key waveforms of the proposed SSFB converter.

approximately by $\frac{1}{2\pi\sqrt{L_o C_{\text{clamp}}}}$. The voltage across the diode D_5, v_{D5}, is decreased as the clamping capacitor is charged, which can be expressed by

$$v_{D5}(t) \approx nV_s - v_{C\_\text{clamp}}(t_1) - i_{C\_\text{clamp}}(t_1)\sqrt{\frac{L_o}{C_{\text{clamp}}}}\sin\left(\frac{t-t_1}{\sqrt{L_o C_{\text{clamp}}}}\right) \tag{2}$$

where $i_{C\_\text{clamp}}(t_1)$ is equal to the maximum output inductor current $I_{Lo\_\max}$.

At t_2, the voltage v_{D5} reaches zero volts since the clamping capacitor voltage v_{C_clamp} becomes equal to the rectifier voltage v_{rect}. Hence, the time for Mode 2, $t_{\text{mode 2}}$, can be expressed as (3) using (2)

$$t_{\text{mode 2}} = t_2 - t_1 = \sqrt{L_o C_{\text{clamp}}} \arcsin\left(\frac{nV_s - v_{C\_\text{clamp}}(t_1)}{I_{Lo\_\max}}\sqrt{\frac{C_{\text{clamp}}}{L_o}}\right). \tag{3}$$

The output inductor current starts to freewheel with a slope expressed by

$$\frac{di_{Lo}}{dt} = \frac{nV_s - v_{C\_\text{clamp}} - V_o}{L_o}. \tag{4}$$

Mode 3 $[t_2$–$t_3]$: At t_2, since the output inductor current freewheels, the diode D_5 is forward biased and the current

commutation occurs from the rectifier diodes D_1 and D_4 to the diode D_5. Consequently, the rectifier voltage $v_{\rm rect}$ is equal to the clamping capacitor voltage $v_{C\_\rm clamp}$. The current of the diode D_5 slowly increases after the voltage across it becomes zero, thereby achieving ZCS turn on for the diode D_5 , as shown in Fig. 4. Here, the clamping capacitor $C_{\rm clamp}$ starts to resonate with only the leakage inductance of the transformer $L_{\rm lk}$ because the freewheeling current of the transformer flows through the diodes D_5 and D_6. The current of the clamping capacitor $C_{\rm clamp}$ during this mode can be expressed by

$$i_{C\_\rm clamp}\ (t) = i_{C\_\rm clamp}\ (t_2)\cos\left(\frac{t-t_2}{\sqrt{n^2L_{\rm lk}C_{\rm clamp}}}\right) + (nV_s - v_{C\_\rm clamp}\,(t_2))\sqrt{\frac{n^2L_{\rm lk}}{C_{\rm clamp}}}\sin\left(\frac{t-t_2}{\sqrt{n^2L_{\rm lk}C_{\rm clamp}}}\right). \tag{5}$$

Therefore, the clamping capacitor voltage $v_{C\_\rm clamp}$ can be expressed by

$$v_{C\_\rm clamp}\ (t) = nV_s\ + (v_{C\_\rm clamp}\,(t_2) - nV_s) \times \cos\left(\frac{t-t_2}{\sqrt{n^2L_{\rm lk}C_{\rm clamp}}}\right) + i_{C\_\rm clamp}\,(t_2)\sqrt{\frac{n^2L_{\rm lk}}{C_{\rm clamp}}} \times \sin\left(\frac{t-t_2}{\sqrt{n^2L_{\rm lk}C_{\rm clamp}}}\right). \tag{6}$$

It can be seen in (6) that a larger leakage inductance value of the transformer results in a higher clamping capacitor voltage. Unlike the conventional PSFB converter, since the leakage inductance value of the transformer has no relationship with the ZVS condition of the primary switches in the proposed converter, it is desirable to design the transformer to have as small a leakage inductance as possible.

At the end of commutation, the current flowing through the rectifier diodes D_1 and D_4 decays to zero and the value of the primary current $i_{\rm Pri}$ becomes equal to that of the magnetizing current i_{Lm} of the transformer at t_3. Since $i_{C\_\rm clamp}\ (t_3) = 0$, the time period for Mode 3 $t_{\rm mode\ 3}$ can be calculated as (7) by using (5)

$$t_{\rm mode\ 3} = t_3\ -\ t_2 = \sqrt{n^2L_{\rm lk}C_{\rm clamp}}\ \arctan\left(\frac{i_{C\_\rm clamp}\,(t_2)}{(nV_s - v_{C\rm clamp}\,(t_2))\sqrt{\frac{n^2L_{\rm lk}}{C_{\rm clamp}}}}\right). \tag{7}$$

Since $nV_s = v_{C\_\rm clamp}\ (t_2)$, $t_{\rm mode\ 3}$ can be calculated by $\frac{\pi}{2}\sqrt{n^2L_{\rm lk}C_{\rm clamp}}$. Therefore, the total charge time of the clamping capacitor $C_{\rm clamp}$ can be expressed by

$$t_{C\_\rm clamp} = t_{\rm mode\ 2}\ + t_{\rm mode\ 3}. \tag{8}$$

The output inductor current continues to freewheel with a slope expressed by

$$\frac{di_{Lo}}{dt} = \frac{-V_o}{L_o}\ . \tag{9}$$

At first glance, the slope of the output inductor current in (9) looks different from that in (4). However, both of them have the same values since the clamping capacitor voltage and the reflected primary voltage are the same in value during Mode 3.

Mode 4 [t_3–t_4]: Only a small magnetizing current i_{Lm} flows in the primary side of the converter during this interval, thereby achieving the ZCS condition for the primary switches and rectifier diodes at t_4. At the secondary side, D_5 and D_6 participate in constituting a closed loop for the freewheeling current.

Mode 5 [t_4–t_5]: This mode begins when the switches $\rm S_1$ and $\rm S_4$ are turned off at t_4. Since the magnetizing current i_{Lm} starts to charge the output capacitors of the switches $\rm S_1$ and $\rm S_4$ and to discharge the output capacitors of the switches $\rm S_2$ and $\rm S_3$, the voltages across the switches $\rm S_2$ and $\rm S_3$ are decreased to zero volts. Since $i_{\rm Pri}$ flows through the body diodes of $\rm S_2$ and $\rm S_3$ before the switches are turned on, the ZVS turn-on condition can be achieved in this mode. The rectifier voltage $v_{\rm Rect}$ and the secondary switch voltage v_{DS_Q1} are still clamped by the clamping capacitor voltage $C_{\rm clamp}$ during this mode.

Mode 6 [t_5–t_6]: At t_5, switches $\rm S_2$, $\rm S_3$, and $\rm Q_1$ turn ON simultaneously. The clamping capacitor $C_{\rm clamp}$ discharges the absorbed energy to the load. Resonance occurs between the clamping capacitor $C_{\rm clamp}$ and the output inductor L_o. Hence, the voltage of the clamping capacitor $V_{C\rm clamp}$ is gradually decreased by

$$v_{C\_\rm clamp}\ (t) = v_{C\_\rm clamp}\ (t_5) - i_{C\_\rm clamp}\,(t_5)\sqrt{\frac{L_o}{C_{\rm clamp}}}\sin\left(\frac{t-t_5}{\sqrt{L_oC_{\rm clamp}}}\right) \tag{10}$$

where $i_{C\_\rm clamp}(t_5) \approx I_{Lo} - \frac{\Delta I_{Lo}}{2}$

Since the clamping capacitor voltage is still higher than the voltage at the secondary winding of the transformer, $v_{C\_\rm clamp} > nV_s$, power cannot be transferred to the secondary side even though the switches $\rm S_2$ and $\rm S_3$ are already turned ON. Therefore, only the stored energy $C_{\rm clamp}$ is transferred to the load. This is the principle of the nondissipative snubber. Since this clamping capacitor is working as a voltage source during Mode 6 and the subsequent Mode 7, the energy transfer continues as soon as the secondary switch $\rm Q_1$ is turned ON. Hence, there is no duty loss in the proposed SSFB converter.

This mode ends when $v_{C\_\rm clamp}$ becomes equal to nV_s at t_6. The output inductor current starts to increase with a slope expressed by

$$\frac{di_{Lo}}{dt} = \frac{v_{C\_\rm clamp}\,(t_5)\ - V_o}{L_o}\ . \tag{11}$$

Mode 7 [t_6–t_7]: At t_6, the value of $i_{\rm Pri}$ reverses its direction and starts to transfer power to the secondary side through the rectifier diodes D_2 and D_3. The resonance started in the previous mode continues, and the clamping capacitor $C_{\rm clamp}$ is fully discharged at t_7. In the meantime, the primary current increases and reaches the reflected output inductor current at t_7, and the converter becomes ready to transfer power to the load.

After Mode 7, the other half of the switching cycle starts and the circuit works the same way as in the first half-switching cycle except for the current direction.

III. Analysis of the Proposed SSFB Converter

A. ZVS Turn On for All of the Primary Switches Over the Entire Load Range

For the simplicity of the analysis, it is assumed that the output capacitors C_{OSS} for all of the primary switches have the same value of capacitance and that the magnetizing current is constant during the time between t_3 and t_4. During the time in Mode 5, the primary side of the proposed SSFB converter is isolated from the secondary side since the freewheeling current of the output inductor flows through the diodes D_5 and $D_{6,}$ as shown in Fig. 3(e). Hence, the ZVS condition for the primary switches during the dead time is achieved by the inductive energy stored in the primary side only. In order to achieve the ZVS condition for the primary switches, the energy stored in the magnetizing inductance L_m and the leakage inductance $L_{\rm lk}$ of the transformer $E_{\rm ZVS}$ must be sufficient to fully charge the C_{OSS} of one pair of switches and to fully discharge that of the other pair. As long as the transformer is designed to satisfy the condition in (12), the ZVS for the primary switches of the proposed SSFB converter can be achieved regardless of the load since $L_m \gg L_{\rm lk}$

$$E_{\rm ZVS} = \frac{1}{2} L_m I_m^2 > \frac{1}{2} (4 \times C_{oss}) V_{\rm in}^2 \tag{12}$$

where I_m is the amplitude of the magnetizing current in the transformer that can be calculated by (13), where *fs* is the switching frequency of the secondary switch Q_1

$$I_m = \frac{V_s}{4 f_s L_m} . \tag{13}$$

By substituting (12) into (13), the magnetizing inductance of the transformer L_m can be calculated as

$$L_m < \frac{1}{64 f_s^2 C_{OSS}}. \tag{14}$$

Hence, in order to guarantee the ZVS operation for all of the primary switches, the minimum dead time $t_{\rm dead}$ to charge and discharge the four output capacitors of the switches should satisfy

$$t_{\rm dead} > \frac{4 C_{oss} V_s}{I_m} = 16 C_{oss} L_m f_s. \tag{15}$$

B. ZCS Turn Off for All of the Primary Switches

In case of the conventional PSFB converter, the main switching loss is caused by the hard-switching turn off for all of the primary-side switches, and it is especially severe at a full load. Both the lagging legs and the leading legs turn off with the reflected output inductor current, thereby contributing to a higher loss and a lower power conversion efficiency. However, in the proposed converter, ZCS turn off is possible for all of the primary switches since the secondary switch Q_1 turns off earlier than the primary switches. During the time $t_{\rm ZCS}$ in Fig. 4, the primary current is decreased and its amplitude becomes equal to that of the small magnetizing current. Therefore, the turn-off loss for all of the primary switches is negligible. In order to achieve the ZCS condition for the primary switches, the minimum time $t_{\rm ZCS}$ should be larger than the total charge time for the clamping capacitor as shown in

$$t_{\rm ZCS} > t_{C\_\rm clamp}. \tag{16}$$

C. ZCS Turn On and ZCS Turn Off for the Rectifier Diodes and D_5, and Elimination of the Reverse-Recovery Problems

It is possible to achieve both ZCS turn on and ZCS turn off for the secondary rectifier diodes and the diode D_5 in the proposed SSFB converter. As explained in the previous chapter, the bias conditions for the secondary rectifier diodes and the diode D_5 are decided by the clamping capacitor voltage, and the current commutation occurs only after the forward bias condition is achieved. Therefore, perfect soft switching is possible for the secondary rectifier diodes and the diode D_5. The reverse-recovery losses of the diodes can be eliminated due to the ZCS turn-off characteristics of the proposed converter. However, in case of the diode D_6, soft switching is not possible because its bias condition is determined by the switching of the secondary switch Q_1 and the clamp capacitor. Since the clamping capacitor voltage changes gradually, switching loss cannot be avoided.

D. Voltage Gain of the Proposed SSFB Converter and Its Inherent No Duty-Cycle Loss Characteristics

As shown in Fig. 3, the output inductor current increases during Mode 1, Mode 6, and Mode 7, and decreases from Mode 2 to Mode 5. Hence, the voltage gain of the proposed SSFB converter can be determined by using the volt–second balance principle with (1), (9), and (11)

$$\frac{V_{C\_\rm clamp} - V_o}{L_o} D_1 + \frac{n V_s - V_o}{L_o} D_2 = \frac{V_o}{L_o} (1 - D_1 - D_2) \tag{17}$$

where $D_1 = (t_7 - t_5)/T_S, D_2 = (t_1 - t_0)/T_S,$ and T_S (= 1/*fs*) is the switching period of the secondary switch Q_1.

Then, the output voltage can be represented by using

$$V_o = V_{C\_\rm clamp} D_1 + n V_s D_2. \tag{18}$$

Since the average value of the clamping capacitor voltage during the time (t_5–t_7) is the same as that of the reflected primary voltage nV_s and the duty of the secondary switch $D = D_1 + D_2$, the voltage gain of the proposed SSFB converter can be written by

$$\frac{V_o}{V_s} = n(D_1 + D_2) = nD. \tag{19}$$

Unlike the conventional PSFB converter, there is no duty-cycle loss in the proposed SSFB converter. In the conventional PSFB converter, since the duty-cycle loss occurs during the time for the primary current to change its direction, it causes a reduction in the output voltage, and no power transfer occurs during this period. Hence, this results in an increase in the turns ratio of the transformer to obtain a required output voltage. However, in the proposed SSFB converter, the clamping capacitor $C_{\rm clamp}$ is charged during the time (t_1–t_3) after the secondary switch Q_1 is turned OFF, and it is discharged during the time (t_5–t_7) after the secondary switch Q_1 is turned ON. Since the clamping capacitor $C_{\rm clamp}$ works as a voltage source during the time

(t_5–t_7), the duty-cycle loss does not exist in the proposed converter. Therefore, it has a higher dc conversion ratio compared with that of the conventional PSFB converter.

The current ripple of the output inductor ΔI_{Lo} and the voltage ripple of the output capacitor ΔV_O can be calculated by using (20) and (21), respectively. Since there is no duty loss, both of the ripple values in (20) and (21) are smaller than those of the conventional PSFB converter

$$\Delta I_{Lo} = \frac{V_o\,(1\ -\ D)\,T_s}{L_o} \tag{20}$$

$$\Delta V_O = \frac{V_o\,(1\ -\ D)\,T_s^2}{8C_oL_o}\,. \tag{21}$$

E. Voltage Ringing at the Secondary Switch and the Nondissipated CDD Turn-Off Snubber

In this section, the effectiveness of the CDD snubber to damp the voltage ringing across the secondary rectifier diode and the secondary switch is presented. Due to the difference in the primary-side switching scheme, the principle behind the voltage oscillation of the proposed SSFB converter is different from that of the PSFB converter.

In the conventional PSFB converter, the voltage ringing across the rectifier diodes occurs due to the resonance between the leakage inductance of the transformer and the junction capacitance of the rectifier. It occurs when the primary current reaches the reflected output inductor current after the commutation of the rectifier diodes. It is well known that since the voltage across the transformer secondary winding is equal to zero and the output inductor current is at its minimum value, the peak value of the ringing voltage is twice the input voltage [11].

However, in the SSFB converter with no snubber shown in Fig. 1, a voltage ringing occurs right after the secondary switch Q_1 is turned off. It is caused by the resonance between the leakage inductance of the transformer and the effective capacitance $C_{\rm eff}$, which is a combination of the junction capacitances of the rectifier diodes and the output capacitance of the secondary switch. At this moment, since the voltage of the secondary winding of the transformer is equal to nV_s and the output inductor current is at its maximum value $I_{Lo\_\max}$, the voltage ringing of the SSFB converter in Fig. 1 is far more severe compared with the conventional PSFB converter.

The inductive energy stored in the leakage inductance reflected to the secondary side $W_{L\_\rm lk}$ can be expressed by

$$W_{L\_\rm lk} = \frac{1}{2}\,n^2L_{\rm lk}I_{Lo\_\max}^2. \tag{22}$$

The relationship between the increase in the capacitive energy $\Delta W_{c\_\rm eff}$ and that in the voltage ΔU can be expressed by

$$\Delta W_{c\_\rm eff} = \frac{1}{2}\,C_{\rm eff}\,\Delta U^2. \tag{23}$$

When the switch Q_1 is turned OFF, the voltage rise of the effective capacitance ΔU can be easily derived as in (24) by using (22) and (23)

$$\Delta U\ = nI_{Lo(\max)}\sqrt{\frac{L_{\rm lk}}{C_{\rm eff}}}. \tag{24}$$

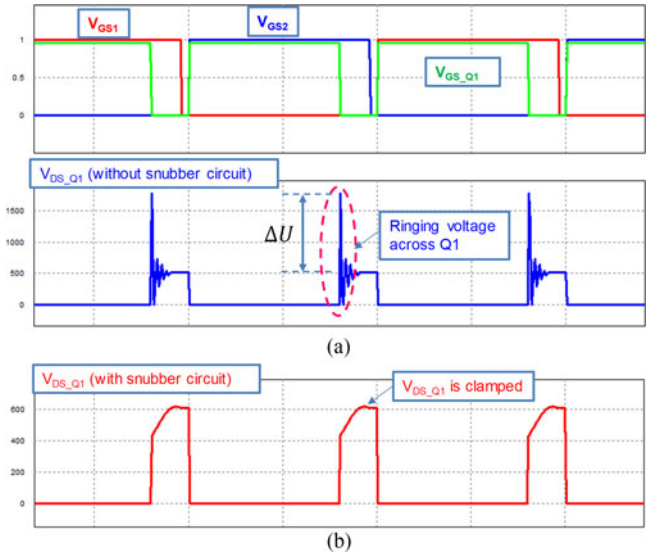

Fig. 5. Voltage ringing across the switch Q_1. (a) Converter in Fig. 1. (b) Proposed SSFB converter in Fig. 2.

Since the effective capacitance $C_{\rm eff}$ is very small, the voltage imposed to the secondary switch Q_1 increases drastically in a short period of time, as shown in Fig. 5(a). In order to deal with this issue, the proposed SSFB converter has adopted a nondissipative CDD snubber as shown in Fig. 2. The ringing voltage can be suppressed, as shown in Fig. 5(b), and its peak value can be calculated by using (6).

The employed CDD snubber circuit introduces several advantages for the proposed SSFB converter as follows. 1) When the switch Q_1 is turned OFF, the clamping capacitor $C_{\rm clamp}$ absorbs the inductive energy from the primary side and transfers it to the load, thereby acting as a nondissipative snubber. 2) It also clamps the voltage across the rectifier diodes, the diodes D_5 and D_6, and the secondary switch Q_1. 3) The clamping capacitor $C_{\rm clamp}$ helps reset the primary current of the transformer, thereby achieving the ZCS condition for the primary switches. 4) When the diodes D_5 and D_6 work as a snubber, it also constitutes a freewheeling current path. Hence, it contributes to a reduction in the component count since a separate freewheeling diode is not required.

IV. Experimental Results and Discussions

A 3-kW prototype circuit has been implemented, as shown in Fig. 6, and tested to verify the operation principle and the performance of the proposed converter. Table II shows the specification of the proposed SSFB converter, and Table III shows the components used for the prototype converter.

Fig. 7(a) and (b) shows that the waveforms of the primary switch S_1 and the rectifier diode D_1 that can achieve ZVS turn on and ZCS turn off. Thanks to the ZCS turn off of the rectifier diode, there is no reverse-recovery problem in the proposed converter. Fig. 7(c) shows that the voltage of the secondary switch Q_1 is successfully clamped to 610 V by the nondissipative snubber.

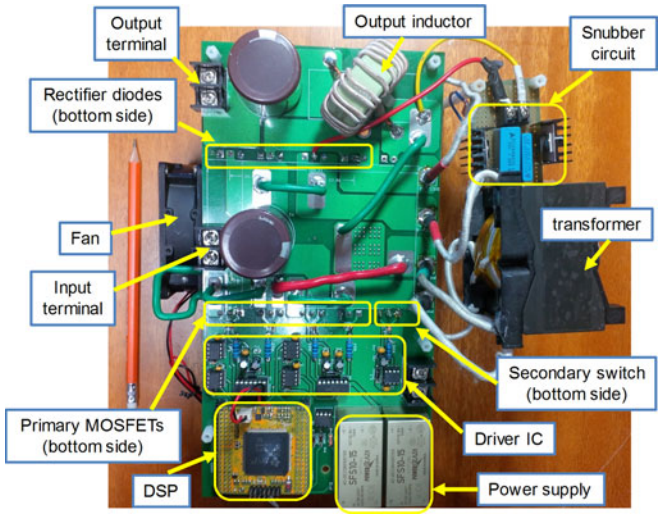

Fig. 6. Photograph of the proposed converter prototype.

TABLE II
SPECIFICATION OF THE PROPOSED CONVERTER

Parameter	Nomenclature	Value
Nominal input voltage	V_s	200 V
Nominal output voltage	V_o	400 V
Maximum output power	$P_{o,\max}$	3 kW
Primary switching frequency	$f_{s,\mathrm{pri}}$	50 kHz
Secondary switching frequency	$f_{s,\mathrm{sec}}$	100 kHz
Turn ratio of the SSFB transformer	$1:n$	1:2.5
Magnetizing inductance	L_m	765 μH
Leakage inductance	L_{lk}	2 μH
Clamping capacitor	C_{clamp}	25 n F
Output inductor	L_O	500 μH

TABLE III
COMPONENTS USED IN THE PROTOTYPE CONVERTER

Component	Manufacturer	Part #
Primary-side MOSFET	Infineon	IPP220N25NFD
Secondary-side MOSFET	Fairchild	FCH041N65F
Diode rectifiers	Vishay	HFA50PA60
Snubber film capacitors	Avago	Z112688575 (22 nF) N113152287 (4.7 nF)

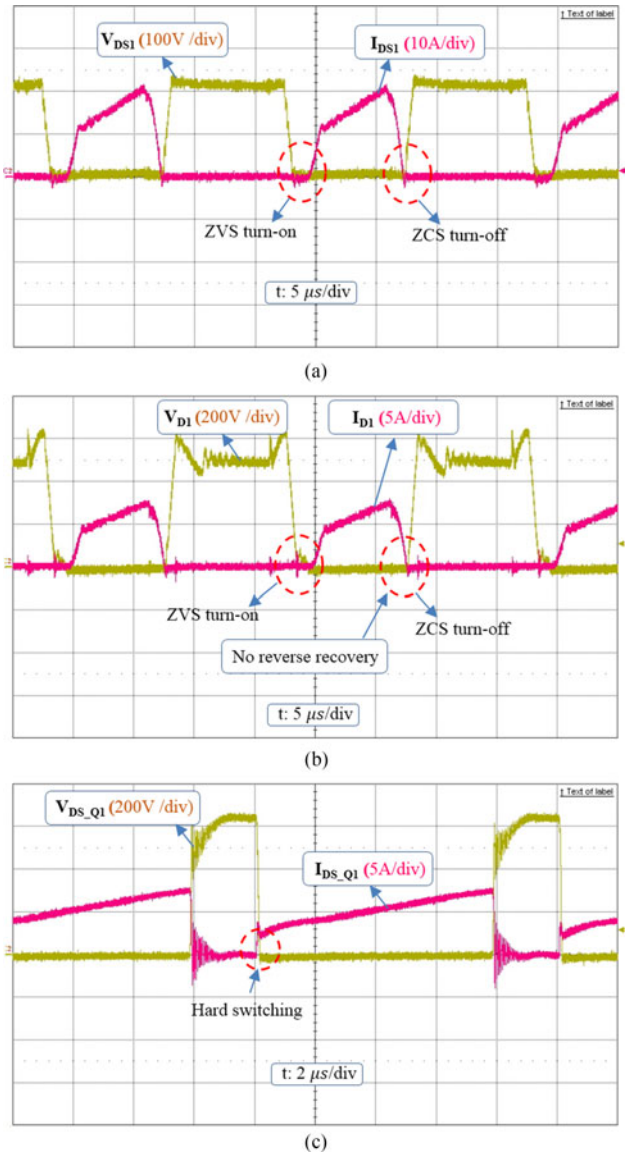

Fig. 7. Experimental waveforms at 2-kW output power. (a) Primary side switch S_1. (b) Rectifier diode D_1. (c) Secondary side switch Q_1.

Fig. 8 shows voltage and current waveforms of the three components in the snubber circuit. In Fig. 8(a), the clamping capacitor C_{clamp} is charged to the peak value of 610 V due to resonance. This energy is transferred to the output through the diode D_5 which can achieve ZCS turn on and ZCS turn off, as shown in Fig. 8(b). Although the diode D_6 operates under hard switching, its voltage is also clamped to 610 V, as shown in Fig. 8(c).

Fig. 9 shows the experimental results at the light-load condition (300 W, 10% load). As shown in Fig. 9(a), the ZVS turn on of the primary switch at the light-load condition is achieved without difficulty since the transformer is designed to have a sufficient magnetizing inductance to discharge the output capacitances of the MOSFETs regardless of the load during the deadtime. Fig. 9(b) shows the soft switching of the rectifier diodes in the proposed converter. This can be achieved perfectly even at the light-load condition. Fig. 9(c) shows waveforms at the secondary switch. It operates under the hard-switching condition and it is one of the major losses of the converter.

In order to show the superiority of the proposed SSFB converter over the conventional PSFB converter, the efficiency of each converter is plotted, as shown in Fig. 10. After the efficiency of the proposed SSFB converter is measured, the conventional PSFB converter is implemented by disabling the secondary switch and the CDD snubber circuit in the proposed converter is used to measure the efficiency.

The measured efficiency curve of the proposed SSFB converter with a 200-V input and a 400-V output is drawn over the wide load range from 300 W to 3 kW, as shown in Fig. 11. A maximum efficiency of 96% is achieved at a 500-W output with the proposed converter. At a light load, the efficiency of the proposed converter is much higher than that of the conventional PSFB converter. This is attributed to the full soft switching of the primary switches and rectifier diodes, the inherent circulating

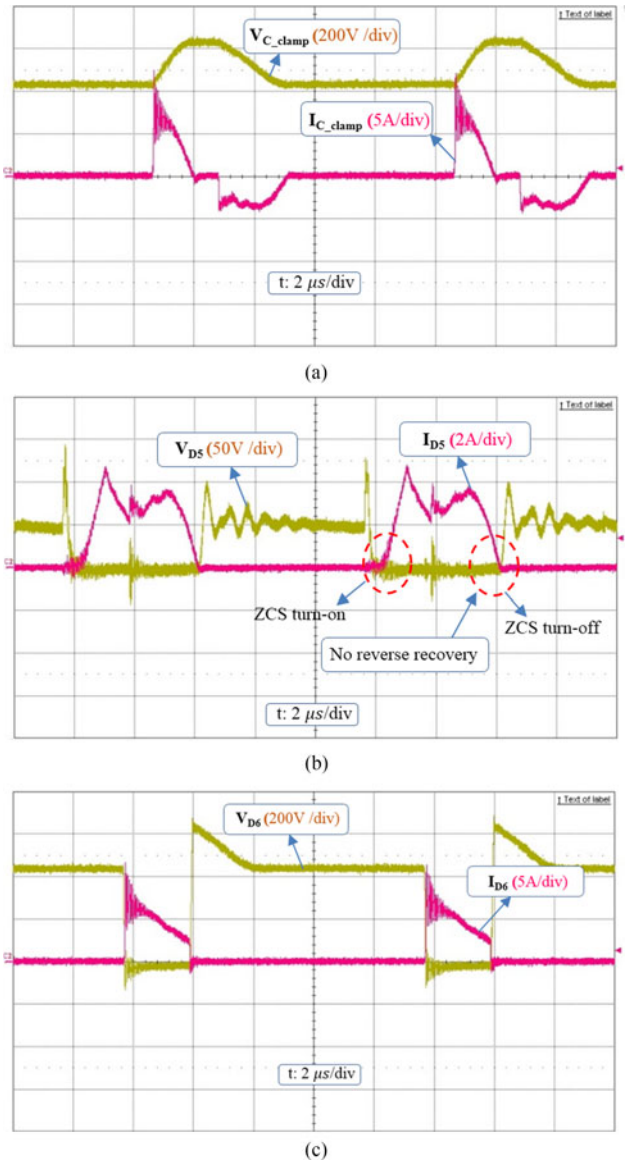

Fig. 8. Experimental waveforms of snubber circuit at 2 kW. (a) Clamping capacitor C_{clamp}. (b) Diode D_5. (c) Diode D_6.

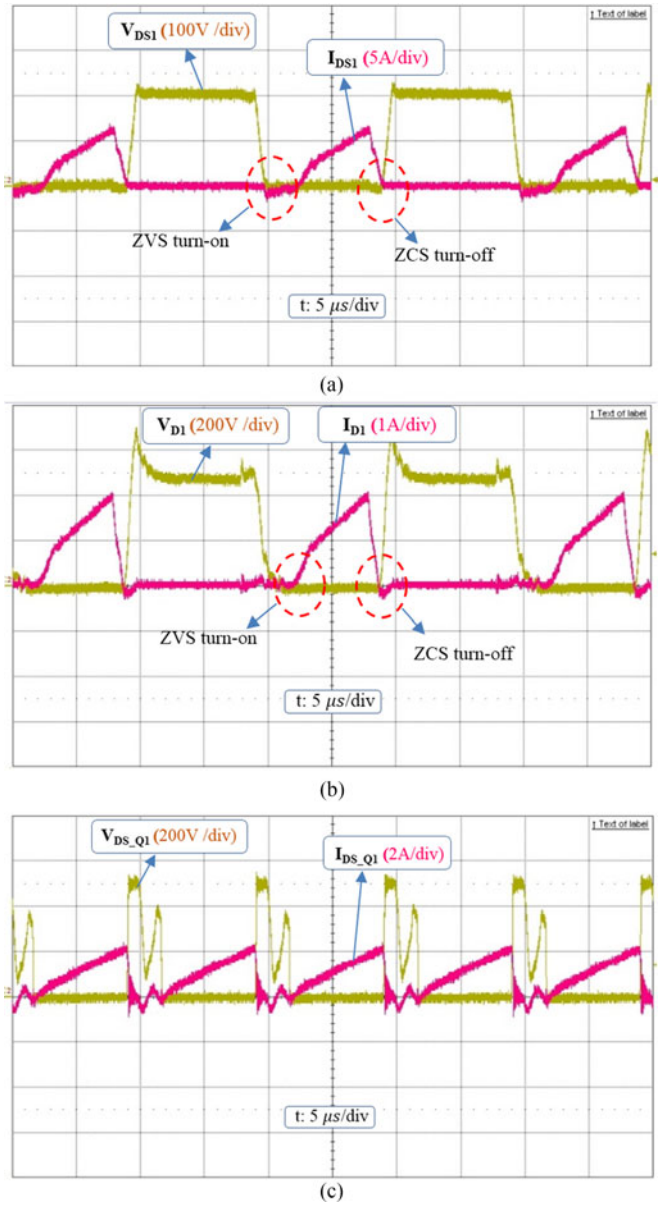

Fig. 9. Experimental waveforms at 300-W load. (a) Primary-side switch S_1. (b) Rectifier diode D_1. (c) Secondary-side switch Q_1.

current free characteristics, and the nondissipative snubber of the proposed SSFB converter. When the power is increased, the efficiency of the proposed converter becomes similar to that of the conventional PSFB converter due to an increase in the hard-switching losses at the secondary-side switch and the diode D_6.

Fig. 11 shows a loss analysis of the proposed converter and the conventional PSFB converter under different load conditions. All the equations and parameters used for the calculation can be found in the Appendix. A significant difference between the two converters can be found in terms of the losses caused by the switches and diodes as expected. Though the losses of two converters are similar at heavy load, the loss of the proposed converter at light load is significantly lower than that of the conventional PSFB converter. This kind of characteristics in power supply system is very important if the recent trend in power supply efficiency such as 80 Plus certification program is considered.

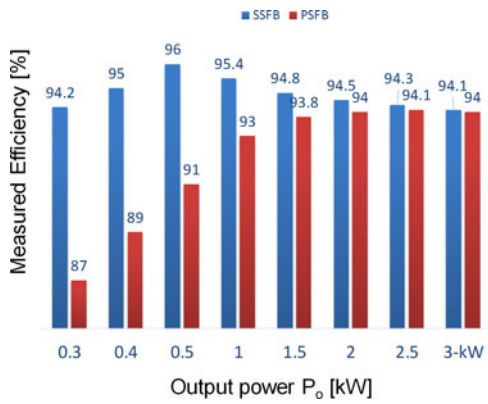

Fig. 10. Efficiency comparison between the conventional PSFB and the proposed SSFB converter.

TABLE IV
COMPARISON OF THE DIFFERENT KINDS OF FULL-BRIDGE CONVERTER TOPOLOGIES IN TERMS OF THE VOLTAGE STRESS OF THE RECTIFIER DIODES AND THE EFFICIENCY

Reference	Maximum voltage stress on the rectifier diode	Calculated maximum voltage stress on the rectifier diode with $V_s = 200$ V, $V_O = 400$ V, and $n = 2.5$	Efficiency of the converter shown in the reference			
			at 10% load	at 50% load	at 100% load	Maximum efficiency
Kim *et al.* [13]	$2nV_s$	1000 V	89%	96%	94.8%	96.5%
Cho *et al.* [14]	$2nV_s - V_O$	600 V	86%	95%	95%	95%
Kim and Kim [20]	$nV_s + V_O$	900 V	N/A	N/A	N/A	N/A
Wu *et al.* [21]	$\frac{3V_O}{2}$	600 V	88%	94.8%	94.5%	94.8%
Song and Huang [22]	$2V_O$	800 V	N/A	N/A	N/A	N/A
Proposed converter	$nV_s + I_{Lo(\max)}\sqrt{\frac{n^2 L_{lk}}{C_{\text{eff}}}}$	610 V	94.2%	94.8%	94.1%	96%

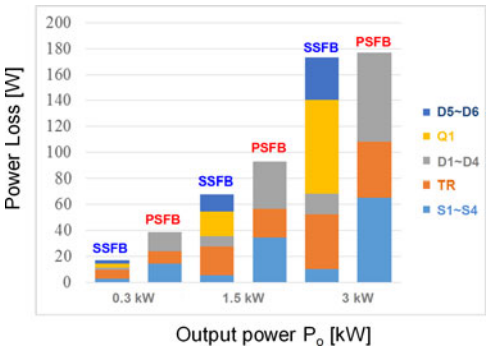

Fig. 11. Loss analysis of the proposed SSFB converter and the conventional PSFB converter.

It can be realized from the loss breakdown graph in Fig. 11 that the efficiency of the proposed SSFB converter can be further improved if a soft-switching technique for the secondary switch is adopted. Various feasible solutions can be considered to obtain a soft-switching condition for the additional switch, and, hence, a higher efficiency at heavy load. Some approaches based on a tapped-inductor [27] or a coupled-inductor [28], [29] could be a good candidate to obtain soft-switching conditions for the secondary switch.

Table IV shows the performance comparison between the conventional zero-voltage zero-current switching full-bridge converters and the proposed converter in terms of the voltage stress of the rectifier diodes and the efficiency. It can be noticed from Table IV that the proposed converter exhibits excellent characteristics in terms of the voltage stress of the rectifier diodes, the light load efficiency, and the maximum efficiency.

V. CONCLUSION

In this paper, a new SSFB dc–dc converter is introduced. By employing an additional switch and a nondissipative snubber circuit, the proposed SSFB converter has the following advantages over the conventional PSFB converter. 1) ZVS turn on and ZCS turn off for all of the primary switches over the entire load range. 2) ZCS turn on and ZCS turn off for all of the rectifier and a snubber diode, and the elimination of their reverse-recovery problem. 3) Inherent circulating current free characteristics and no conduction losses associated with it. 4) No duty-cycle loss due to the energy transfer by the clamp capacitor. 5) High efficiency especially at light loads. 6) A simple switching and control scheme. The loss associated with the secondary-side switch is a sole disadvantage of the proposed converter; hence, the proposed converter is more suitable for voltage step-up applications than the voltage step-down applications of which output currents are large. However, if a widebandgap device, such as SiC or GaN, is employed for the secondary switch, the efficiency of the proposed converter can be further improved.

APPENDIX

TABLE V
COMPONENT PARAMETERS USED TO CALCULATE LOSSES

Switching parameters	
Primary switching frequency f_{sw}	50 kHz
Duty cycle D_{eff}	0.8
Turn-on time t_{on}	84 ns
Turn-off time t_{off}	84 ns
Primary-side MOSFET	
Part number	220N25NP
$R_{\text{DS(on)}}$	0.022 Ω
Transformer	
Resistance of primary winding $R_{\text{Pri\_SSFB}}$	0.05 Ω
Resistance of secondary winding $R_{\text{Sec\_SSFB}}$	0.1 Ω
Geometry constant of core K_{fe}	7.6
Variation in flux density ΔB	0.32 T
Exponential constant β	2.6
Cross sectional area of core A_C	4 cm^2
Magnetic path length of core l_m	20 cm
Secondary Rectifier Diodes	
Part number	HFA50PA60
Forward voltage V_F	1.3 V
Switch Q_1	
Part number	FCH041N65F
$R_{\text{DS(on)}}$	0.036 Ω
Diode D_5	
Part number	HFA50PA60
Forward voltage V_F	1.3 V
Diode D_6	
Part number	HFA50PA60
Forward voltage V_F	1.3 V

TABLE VI
COMPARISON OF LOSS ANALYSIS BETWEEN SSFB CONVERTER AND PSFB CONVERTER

Component	Loss	SSFB converter	PSFB converter	Nomenclature
Primary MOSFETs	Conduction loss	$P_{Switch\_cond} = \frac{1}{2} I_{DS}^2 R_{DS(on)}$ / *4 switches*		$\boldsymbol{I_{DS}}$ (A): RMS value of drain-to-source current through MOSFET. $\boldsymbol{R_{DS(on)}}$ (Ω): on-state resistance of the MOSFET.
	Switching loss	-	$P_{Leading\_sw(off)} = \frac{1}{2} V_{in} I_{pp} t_f f_{sw}$ / *2 leading leg switches*; $P_{Lagging\_sw(off)} = \frac{1}{2} V_{in} I_{p2} t_f f_{sw}$ / *2 lagging leg switches*	$\boldsymbol{V_{in}}$ (V): input voltage $\boldsymbol{I_{pp}}$ (A): peak value of primary current in PSFB. $\boldsymbol{I_{p2}}$ (A): value of primary current when the lagging leg switch is off. $\boldsymbol{t_f}$ (s): falling time of the MOSFET $\boldsymbol{f_{sw}}$ (Hz): switching frequency
Transformer	Conduction loss	$P_{XFM\_cond} = (I_{Pri}^2 R_{Pri} + I_O^2 R_{Sec}) D$	$P_{XFM\_cond} = I_{Pri}^2 R_{Pri} + 2 I_D^2 R_{Sec}$	$\boldsymbol{R_{Pri}}$ (Ω): the resistance of the primary winding of transformer. $\boldsymbol{R_{Sec}}$ (Ω): the resistance of the secondary winding of transformer. $\boldsymbol{I_{Pri}}$ (A): RMS value of primary current. $\boldsymbol{I_D}$ (A): RMS current through the diode. $\boldsymbol{K_{fe}}$,$\boldsymbol{\beta}$: constants, which are related to material. $\Delta\boldsymbol{B}$ (T): magnetic flux density of core $\boldsymbol{A_C}$ (cm^2): cross–sectional area of core $\boldsymbol{l_m}$ (cm): magnetic path length
	Core loss	$P_{XFM\_core} = K_{fe} (\Delta B)^{\beta} A_C l_m$		
Rectifier diodes	Conduction loss	$P_{Diode\_cond} = \frac{1}{2} V_F I_O D$ / *4 diodes*		$\boldsymbol{D}$ (%): effective duty $\boldsymbol{I_O}$ (A): average output current. $\boldsymbol{V_F}$ (V): forward voltage drop $\boldsymbol{V_{D\_FR}}$ (V): the forward recovery voltage $\boldsymbol{V_{D\_R}}$ (V): the reverse voltage $\boldsymbol{t_{fr}}$ (s): the turn-on recovery time $\boldsymbol{t_{rr}}$ (s): the reverse recovery time
	Switching loss	-	$P_{D\_sw(on)} = \frac{1}{2} V_{D\_FR} I_O t_{fr} f_{sw}$, $P_{D\_sw(off)} = \frac{1}{2} V_{D\_R} I_O t_{rr} f_{sw}$ / *4 diodes*	
Additional MOSFET Q_1	Conduction loss	$P_{Q1\_cond} = I_O^2 R_{DS(on)} D$ / *1 switch*	-	$\boldsymbol{V_{DS\_Q1}}$(V): drain-to-source voltage of Q_1 $\boldsymbol{t_{sw(on)}}$ (s): turn-on time of Q_1 $\boldsymbol{t_{sw(off)}}$ (s): turn-off time of Q_1
	Switching loss	$P_{Q1\_sw(on)} = \frac{1}{2} V_{DS\_Q1} I_O t_{sw(on)} (2 f_{sw})$, $P_{Q1\_sw(off)} = \frac{1}{2} V_{DS\_Q1} I_O t_{sw(off)} (2 f_{sw})$ / *1 switch*	-	
Additional Diode D_5	Conduction loss	$P_{D5\_cond} = V_F I_{D5} (1 - D)$ / *1 diode*	-	$\boldsymbol{I_{D5}}$(A): average current through the diode D_5.
Additional Diode D_6	Conduction loss	$P_{D6\_cond} = V_F I_{D6} (1 - D)$	-	$\boldsymbol{I_{D6}}$ (A): average current through the diode D_6. $\boldsymbol{V_{D6\_FR}}$ (V): the forward recovery voltage of diode D_6 $\boldsymbol{V_{D6\_R}}$ (V): the reverse voltage of diode D_6 $\boldsymbol{t_{fr}}$ (s): the turn-on recovery time $\boldsymbol{t_{rr}}$ (s): the reverse recovery time

REFERENCES

[1] M. Yilmaz and P. T. Krein, "Review of the impact of vehicle-to-grid technologies on distribution systems and utility interfaces," *IEEE Trans. Power Electron.*, vol. 28, no. 12, pp. 5673–5689, Dec. 2013.

[2] M. Yilmaz and P. T. Krein, "Review of battery charge topologies, charging power levels, and infrastructure for plug-in electric and hybrid vehicles," *IEEE Trans. Power Electron.*, vol. 28, no. 5, pp. 2151–2169, May 2013.

[3] R. A. Fisher, K. D. T. Ngo, and M. L. L. Kuo, "500 kHz 250 W DC-DC converter with multiple output controlled by phase-shift PWM and magnetic amplifiers," in *Proc. High Freq. Power Convers. Conf. Rec.*, 1988, pp. 100–110.

[4] K. D. T. Ngo and R. L. Steigerwald, "Full-bridge lossless switching converter," U.S. Patent 4 864 479, Sep. 5, 1989.

[5] V. C. Vlatko *et al.*, "Small-signal analysis of the phase-shifted PWM converter," *IEEE Trans. Power Electron.*, vol. 7, no. 1, pp. 128–135, Jan. 1992.

[6] Y. D. Kim, K. M. Cho, D. Y. Kim, and G. W. Moon, "Wide-range ZVS phase-shift full-bridge converter with reduced conduction loss caused by circulating current," *IEEE Trans. Power Electron.*, vol. 28, no. 7, pp. 3308–3316, Jul. 2013.

[7] B. Y. Chen and Y. S. Lai, "Switching control technique of phase-shift-controlled full-bridge converter to improve efficiency under light-load and standby conditions without additional auxiliary components," *IEEE Trans. Power Electron.*, vol. 25, no. 4, pp. 1001–1012, Apr. 2010.

[8] C. Liu *et al.*, "High-efficiency hybrid full-bridge–half-bridge converter with shared ZVS lagging leg and dual outputs in series," *IEEE Trans. Power Electron.*, vol. 28, no. 2, pp. 849–861, Feb. 2013.

[9] I. O. Lee and G. W. Moon, "Half-bridge integrated ZVS full-bridge converter with reduced conduction loss for electric vehicle battery chargers," *IEEE Trans. Ind. Electron.*, vol. 61, no. 8, pp. 3978–3988, Aug. 2014.

[10] B. Gu, C.-Y. Lin, B. F. Chen, J. Dominic, and J.-S. Lai, "Zero-voltage-switching PWM resonant full-bridge converter with minimized circulating losses and minimal voltage stresses of bridge rectifiers for electric vehicle," *IEEE Trans. Power Electron.*, vol. 28, no. 10, pp. 4657–4667, Oct. 2013.

[11] S.-Y. Lin and C.-L. Chen, "Analysis and design for RCD clamped snubber used in output rectifier of phase-shift full-bridge ZVS converters," *IEEE Trans. Ind. Electron.*, vol. 45, no. 2, pp. 358–359, Apr. 1998.

[12] J.-G. Cho, C.-Y. Jeong, and F. C. Y. Lee, "Zero-voltage and zero-current-switching full-bridge PWM converter using secondary active clamp," *IEEE Trans. Power Electron.*, vol. 13, no. 4, pp. 601–607, Jul. 1998.

[13] E.-S. Kim, K.-Y. Joe, M.-H. Kye, Y.-H. Kim, and B.-D. Yoon, "An improved soft-switching PWM FB DC/DC converter for reducing conduction losses," *IEEE Trans. Power Electron.*, vol. 14, no. 2, pp. 258–264, Mar. 1999.

[14] J.-G. Cho, J.-W. Baek, C.-Y. Jeong, and G.-H. Rim, "Novel zero-voltage and zero-current-switching full-bridge PWM converter using a simple auxiliary circuit," *IEEE Trans. Ind. Appl.*, vol. 35, no. 1, pp. 15–20, Jan./Feb. 1999.

[15] M. Cacciato and A. Consoli, "New regenerative active snubber circuit for ZVS phase shift full bridge converter," in *Proc. 26th Annu. IEEE Appl. Power Electron. Conf. Expo.*, Fort Worth, TX, USA, 2011, pp. 1507–1511.

[16] T. F. Chen and S. Cheng, "A novel zero-voltage zero-current switching full-bridge PWM converter using improved secondary active clamp," in *Proc. IEEE Int. Symp. Ind. Electron.*, Montreal, QC, Canada, 2006, pp. 1683–1687.

[17] J. Dudrik, M. Bodor, and M. Pástor, "Soft-switching full-bridge PWM DC–DC converter with controlled output rectifier and secondary energy recovery turn-off snubber," *IEEE Trans. Power Electron.*, vol. 29, no. 8, pp. 4116–4125, Aug. 2014.

[18] J. Dudrik and N. D. Trip, "Soft-switching PS-PWM DC–DC converter for full-load range applications," *IEEE Trans. Ind. Electron.*, vol. 57, no. 8, pp. 2807–2814, Aug. 2010.

[19] H.-S. Choi, J.-W. Kim, and B. H. Cho, "Novel zero-voltage and zero-current-switching (ZVZCS) full-bridge PWM converter using coupled output inductor," *IEEE Trans. Power Electron.*, vol. 17, no. 5, pp. 641–648, Sep. 2002.

[20] E.-S. Kim and Y.-H. Kim, "A ZVZCS PWM FB DC/DC converter using a modified energy-recovery snubber," *IEEE Trans. Ind. Electron.*, vol. 49, no. 5, pp. 1120–1127, Oct. 2002.

[21] X. Wu, X. Xie, J. Zhang, R. Zhao, and Z. Qian, "Soft switched full bridge DC–DC converter with reduced circulating loss and filter requirement," *IEEE Trans. Power Electron.*, vol. 22, no. 5, pp. 1949–1955, Sep. 2007.

[22] T. T. Song and N. Huang, "A novel zero-voltage and zero-current-switching full-bridge PWM converter," *IEEE Trans. Power Electron.*, vol. 20, no. 2, pp. 286–291, Mar. 2005.

[23] T. Mishima, K. Akamatsu, and M. Nakaoka, "A high frequency-link secondary-side phase-shifted full-range soft-switching PWM DC–DC converter with ZCS active rectifier for EV battery chargers," *IEEE Trans. Power Electron.*, vol. 28, no. 12, pp. 5758–5773, Dec. 2013.

[24] J. Zhang, F. Zhang, X. Xie, D. Jiao, and Z. Qian, "A novel ZVS dc/dc converter for high power applications," *IEEE Trans. Power Electron.*, vol. 19, no. 2, pp. 420–429, Mar. 2004.

[25] K. Harada, Y. Ishihara, and T. Todaka, "Analysis and design of ZVS-PWM half-bridge converter with secondary switches," in *Proc. 26th Annu. IEEE Power Electron. Spec. Conf. Rec.*, Atlanta, GA, USA, 1995, vol. 1, pp. 280–285.

[26] S. Yu, D. D. Tran, H. N. Vu, and W. Choi, "A novel soft switching full bridge DC-DC converter," in *Proc. Power Electron. Annu. Conf.*, Jul. 2015, pp. 175–176.

[27] J. H. Park and B. H. Cho, "Nonisolation soft-switching buck converter with tapped-inductor for wide-input extreme step-down applications," *IEEE Trans. Circuits Syst. I, Reg. Papers*, vol. 54, no. 8, pp. 1809–1818, Aug. 2007.

[28] L. Jiang, C. C. Mi, S. Li, C. Yin, and J. Li, "An improved soft-switching buck converter with coupled inductor," *IEEE Trans. Power Electron.*, vol. 28, no. 11, pp. 4885–4891, Nov. 2013.

[29] F. Marvi, E. Adib, and H. Farzanehfard, "Efficient ZVS synchronous buck converter with extended duty cycle and low-current ripple," *IEEE Trans. Ind. Electron.*, vol. 63, no. 9, pp. 5403–5409, Sep. 2016.

Dai-Duong Tran received the B.Sc. degree in electrical engineering from Hanoi University of Science and Technology, Hanoi, Vietnam, in 2011, and the M.Sc. degree in electrical engineering from Soongsil University, Seoul, South Korea, in 2016. Since January 2017, he has been working toward the Ph.D. degree with the Power Electronics and Electrical Machines team in MOBI Research group, Vrije Universiteit Brussel, Brussels, Belgium.

He was a Researcher with Viettel Research and Development Institute, Hanoi, from 2012 to 2014. His research interests include integrated energy management strategies for (hybrid) electric vehicles (EVs), high-efficiency on-board battery chargers, and power electronics interface for powertrain system of EVs.

Hai-Nam Vu received the B.S. degree in electrical engineering from Hanoi University of Science and Technology, Hanoi, Vietnam, in 2014, and the M.S. degree in electrical engineering from Soongsil University, Seoul, South Korea, in 2017.

His research interests include dc–dc converters dealing with the renewable sources and batteries for energy storage system or hybrid electric vehicles, and soft-switching techniques for the pulse-width modulation/pulse-frequency modulation converters.

Sunho Yu was born in Seoul, South Korea, in 1988. He received the B.S. and M.S. degrees in electrical engineering from Soongsil University, Seoul, in 2013 and 2015, respectively.

Since 2016, he has been a Power Electronics Researcher with LG Electronics, Seoul, Korea. His current research interests include high step-up and bidirectional converter for grid-connected applications, such as PV microinverters; soft-switching techniques for PWM/frequency-modulation converters, and dc–dc converter for electric vehicles.

Woojin Choi (S'00–M'05) was born in Seoul, South Korea, in 1967. He received the B.S. and M.S. degrees in electrical engineering from Soongsil University, Seoul, in 1990 and 1995, respectively, and the Ph.D. degree in electrical engineering from Texas A&M University, College Station, TX, USA, in 2004.

He was a Research Engineer with Daewoo Heavy Industries, Seoul, from 1995 to 1998. In 2005, he joined the School of Electrical Engineering, Soongsil University. His research interests include modeling and control of electrochemical energy sources, such as fuel cells, batteries, and supercapacitors; power conditioning technologies in renewable energy systems; and dc–dc converters for electric vehicles and fuel cells.

Dr. Choi is an Associate Editor of the IEEE TRANSACTIONS ON INDUSTRY APPLICATIONS and a Publication Editor of the *Journal of Power Electronics of the Korean Institute of Power Electronics*.